Primljen / Received: 14.11.2023.
Ispravljen / Corrected: 27.3.2024.
Prihvaćen / Accepted: 3.5.2024.
Dostupno online / Available online: 10.5.2024.

Research on leakage hazards of embankments based on 3D electrical resistivity tomography technology

Authors:

[1] Yuehang Zhao, MSc. CE
2234291813@qq.com

[1] Assoc.Prof. Risheng Wang
990853329@qq.com
Corresponding author

[2] Tao Gao, MCE
18615192466@163.com

[3] Tao Guo, MCE
57541378@qq.com

[3] Xin Guo, MCE
379666343@qq.com

[1] Shandong Jiaotong University, China
Faculty of Transportation and Civil Engineering
[2] Shandong Provincial Transportation Planning and Design Institute Group Co., China
[3] Shandong Yellow River Shuncheng Water Conservancy and Hydropower Engineering Co., China

Research Paper

Yuehang Zhao, Risheng Wang, Tao Gao, Tao Guo, Xin Guo

Research on leakage hazards of embankments based on 3D electrical resistivity tomography technology

Leakage is a common issue in reservoirs; however, accurately detecting its location and seepage diameter can be challenging owing to complex geological conditions. Three-dimensional (3D) resistivity tomography (RT), as opposed to traditional resistivity technology, offers advantages such as high observation density, efficiency, information richness, resolution, and intelligence. This study focuses on the application of 3D RT to diagnose leakage in earth and rock embankment dams. By monitoring the resistance change rate obtained from resistivity image processing, this study accurately assessed the development status of the hidden bodies. This research demonstrates that 3D RT enables rapid comparison of deformation and damage states at different moments, enabling continuous and objective monitoring of earth and rock embankment dams. This technology is comprehensive and provides real-time insights.

Key words:
3D resistivity tomography, electrical resistivity of the soil, embankment, accumulation, leakage

Prethodno priopćenje

Yuehang Zhao, Risheng Wang, Tao Gao, Tao Guo, Xin Guo

Istraživanje opasnosti od curenja kod nasipa temeljeno na 3D električnoj tomografiji

Curenje je čest problem u akumulacijama, ali točno otkrivanje njegove lokacije i promjera može biti izazovno zbog složenih geoloških uvjeta. 3D geoelektrična tomografija, temeljena na mjerenju električnih otpornosti tla, za razliku od tradicionalne tehnologije, nudi prednosti kao što su visoka gustoća mjerenja, učinkovitost, bogatstvo informacija, rezolucija i umjetna inteligencija. Ovaj se rad usredotočuje na primjenu 3D tomografije u dijagnostici curenja kod zemljanih i kamenih nasipa. Praćenjem stope promjene otpornosti dobivene obradom snimljenih profila otpornosti, istraživanje točno procjenjuje razvoj skrivenih oblika. Istraživanje pokazuje da 3D tomografija omogućuje brzu usporedbu deformacijskih stanja i oštećenja u različitim trenucima, omogućujući kontinuirano i objektivno praćenje zemljanih i kamenih nasipa. Ova je tehnologija sveobuhvatna i pruža uvide u stvarnom vremenu.

Ključne riječi:
3D geoelektrična tomografija, električna otpornost tla, nasip, akumulacija, curenje

1. Introduction

Seepage is a critical safety factor affecting the operation of embankment dams, leading to various forms of damage beneath the dam. International water conservancy scientists have been actively researching and applying seepage detection methods in embankment leakage diagnostics [1, 2]. Loke et al. [3] utilised the quasi-Newton method to enhance the computational speed of the least squares method, whereas Chambers [4] employed three-dimensional (3D) resistivity tomography (RT) to assess sand and gravel deposits in rivers, illustrating the rapid advancement and widespread application of RT in this field. Zhou [5] and Song [6] conducted resistivity imaging tests for leakage detection in earth and rock dams and pioneered the use of resistivity for dam hazard detection. Zhao et al.. further explored various methods for diagnosing dam leakage, introduced the concept of joint diagnosis through multiple means, and conducted applied research based on this approach [7-10].

Recent advancements in science and technology have led to the emergence of various new techniques for dam leakage detection [11-13], RRT is widely utilised because of its high efficiency [14-16]. Zhou [17] experimentally compared 2D and 3D electrical resistivity tomography (ERT) and demonstrated that 3D ERT scanning provided significantly higher-resolution effects. Additionally, a research team from the Pacific Northwest Laboratory in the USA utilised ERT to monitor deep subsurface cracks and generated 4D images by measuring the electrical conductivity in rocks over time [18]. Kawaguchi et al. [19] applied 3D RT to spatially measure the temperature of high-temperature molten glass, validating its effectiveness in opaque environments, particularly in scenarios involving highly contaminated flows, gas-liquid two-phase flows with a high void fraction, and conductive fields.

While international scholars have extensively studied resistivity imaging technology [20-22], there is limited research on 3D resistivity chromatography imaging technology and its practical applications in engineering. This study focuses on the application of 3D RT to detect seepage potential in the Shangxishan Reservoir through on-site experimental research. By expanding the resistivity pigment threshold before and after the same potential location and analysing the rate of change of resistance, this study accurately determined the state of dyke seepage prevention and reinforcement. These findings provide a basis for dike reinforcement and further validate the effectiveness of 3D RT in reservoir seepage prevention and reinforcement, demonstrating its superior performance in reservoir leakage detection.

2. Electrical resistivity tomography

RT is a noninvasive geophysical exploration technique that reveals the distribution of underground structures and materials by measuring the underground resistivity distribution. The development of this technology can be traced back to the 1960s when it was primarily used in the field of oil exploration. RT has become widely used with the continuous development of computer technology and imaging algorithms.

2.1. Theory of 3D resistivity tomography

The principle of 3D RT aligns with that of the traditional electrical method, which involves transmitting variations in subsurface materials by injecting electricity into the subsurface and observing the distribution of the resulting electric field. This approach effectively addresses various geological challenges. In comparison, 2D high-density RT still faces certain limitations. For instance, subsurface features may not be accurately captured if measurement lines are not strategically placed, leading to challenges in field testing, particularly in the detection of complex leakage pathways. Additionally, quasi-3D images generated by combining multiple 2D cross sections lack the accuracy of true 3D inversions. The 3D inversion method divides the subsurface into small rectangles, establishes a geoelectric model [24], assigns initial resistivity values to each rectangle, calculates resistivity values through forward modelling, compares theoretical and measured values using the least-squares method, and adjusts the resistivity values accordingly [25, 26]. The objective function F was defined as the basis for this process:

$$F = \sum_{i=1}^{N} \left[\ln \rho_m + \ln \rho_t \right]^2 \quad (1)$$

where ρ_m is the measured resistivity value of the profile and ρ_t is the theoretical resistivity value of the initial model.

The accuracy of the measured resistivity values was compared with theoretical values to assess the results of the inversion calculations. If the requirements were not satisfied, the theoretical values were recalculated until the difference fell within an appropriate range.

2.2. Prospects for the development of electrical resistivity tomography

The advantages of RT include its noninvasiveness, high resolution, high precision, and comprehensiveness. It can effectively map the distribution of underground structures and

materials and serves as a crucial tool for research in geology, environmental studies, and hydrology. The advancement of RT imaging technology is closely linked to ongoing progress in computer technology and imaging algorithms. As computer hardware and software continue to evolve, the speed and accuracy of RT imaging have increased significantly. Additionally, the continuous development of imaging algorithms has played a key role in enhancing RT technology. In recent years, machine-learning-based algorithms have emerged, enabling the training of neural networks to improve imaging accuracy and speed.

In the future, RT technology has significant potential for advancement. As exploration depth and accuracy continue to improve, RT is expected to be widely applied in various sectors, such as petroleum, geology, environmental science, and hydrology. In addition, there is a need for ongoing innovation and enhancement of resistivity chromatography imaging technology to address the challenges posed by complex geological settings and practical applications. Advancements in computer technology and imaging algorithms are expected to further enhance the speed and accuracy of RT imaging and expand its applicability across various fields.

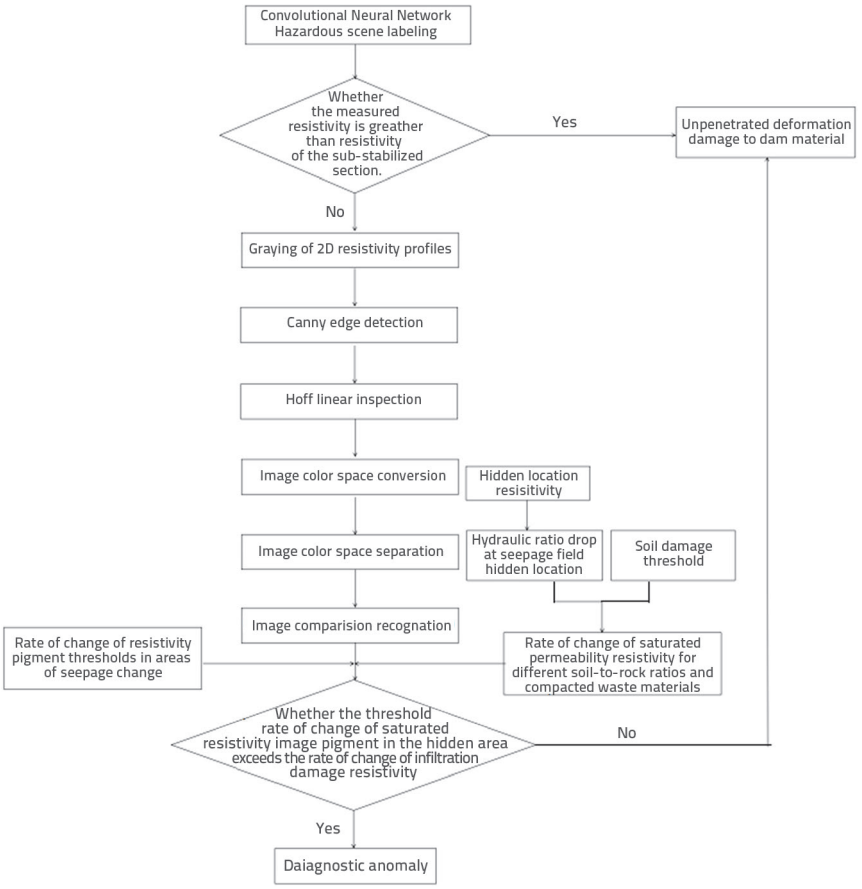

Figure 1. Flow chart for diagnosis of seepage in earth and rock embankment dams

3. Leakage diagnosis process based on 3D electric field distribution of earth and rock embankment dams

Data were collected and transmitted continuously at different time points for 3D resistivity imaging. Using neural network learning to identify hidden dangers, we dissected the locations of these dangers in two dimensions, allowing image comparison sampling. Various techniques such as image grayscale processing, Canny edge detection, Hough straight-line detection, and image colour analysis are employed to analyse pigment changes between images. By comparing the pigment thresholds, the maximum change rate of resistivity in materials with different soil-stone ratios during seepage field evolution can be determined. This analysis helps diagnose potential infiltration damage to soils within the hidden-body extension in the seepage field.

The leakage diagnosis process based on the 3D electric field distribution of earth and rock embankment dams involves a series of steps.

4. Application examples

4.1. Overview of the project

The Shangxishan Reservoir in Qujing City, Yunnan Province, is located beside Shangxishan Village in the Development Zone 10 km west of Qujing City (Figure 2).

Figure 2. Actual view of the project

Figure 3. Map of the current condition of the top, face and back of the earth and rock dams

The Shangxishan Reservoir dam is oriented approximately north-south. The dam crest is covered with a cement-hardened road surface. The side facing the water was sloped at a ratio of 1:2.95, making it relatively flat, and the surface was covered with precast blocks. The side facing away from the water was also sloped, with a slope ratio ranging from 1:2.75 to 1:2.5 and was covered with dense vegetation. Agricultural fields are located below slopes.

The foundation of the Shangxishan Reservoir Dam is situated on Quaternary residual slope deposits and heavily weathered sandstone shale. Because of the loose structural composition of these geological materials, the foundation of the dam lacks stability. In addition, during the dam construction process, various factors such as technological limitations, equipment constraints, and financial considerations influence the choice of materials for the dam body. The dam body predominantly consisted of gravel-containing clay with inadequate compaction density. Consequently, since the completion of the reservoir in 1977, dams and their foundations have frequently experienced seepage issues, which pose a threat to dam safety. According to incomplete records, dozens of instances of seepage have occurred over the past four decades, including two major seepage incidents. While remedial grouting measures were implemented in response to these significant seepage incidents, they were unable to eliminate risks owing to constraints related to funding and technology.

4.2. In-situ electrical testing

4.2.1. On-site electrical testing

Before 2005, two major seepage incidents occurred at the reservoir dam. In response, reservoir management implemented a combination of curtain grouting and concrete impermeable wall treatment to strengthen the dam body. Subsequently, a general raising treatment was applied, which increased the dam body by approximately 1 m. Currently, dam bodies are in a deteriorated state, making it challenging to assess the extent of infiltration damage. Given the poor initial condition of the dam and its extensive treatment history, evaluating the infiltration damage within the dam is complex.

The site investigation found that the dam top along the axial direction of a number of cracks, the surface has been filled with asphalt sealing, the widest cracks up to 2 cm, the height difference between the two sides of 2 ~ 3 cm, micro-surface cracks up to several hundred, the site did not take any treatment measures; dam to the surface of the water surface with prefabricated blocks berms, the site was found to have 4 collapse pit, the largest collapse pit diameter of up to 1 metre, the depth of 12 cm, and part of the collapse pit area of the surface of the prefabricated blocks Lost; dam back water surface is covered by dense weeds, trees, vegetation development is good, in the dam back water surface of the northeast corner of the near mountain there is a place under the weeds of water, recent seepage of good increase, see Figure 3.

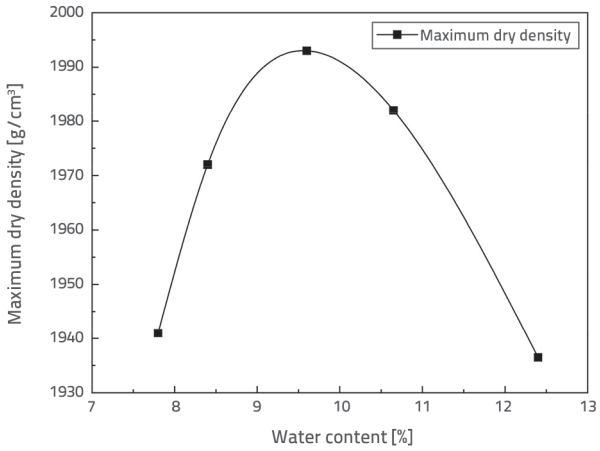

Figure 4. Diagram of soil sample compaction test in the field

After on-site sampling, sieving and percussion test of the soil in the collapsed pit are shown in Figure 4, the maximum dry density of the dam material was obtained as 1.994 g/cm3, the optimum moisture content was 9.6 %,, after sieving and weighing, the soil and rock mass ratio was approximately 7:3, the sieved particle size d10 was obtained from the on-site soil sieving curves as 0.1 mm, d40 as 0.29 mm, d60 as 0.72 mm, and the coefficient of inhomogeneity: $\eta = d_{60}/d_{40} = 0{,}72/0{,}29 = 2{,}48 < 10$. Simulatneously, the exposed part of the soil body of the site dam was levelled and cleaned, and

a compaction test was performed, which showed that the compaction of the dam body was 97.7 %.

4.2.2. Equipment and line layout

A 5 × 5 m grid of uniform electrodes was utilized for the measurements, a technique employed to optimize the monitoring area resolution [23]. The power supply and measurement electrodes were positioned on both slopes of the dam, covering an area of 110 × 145 m. These electrodes, constructed from copper, were linked to the host computer through a 32-core cable. To ensure proper contact between the electrodes and the dam, they were carefully placed using tape. The measurement process involved a four-pole gradient in both inline and crossline directions, with a supply voltage of 288 V.
Considering the field conditions, a 70 × 110 m detection grid was established in the northern section of the dam. This grid extended from the eastern dam water surface to the western slope foot and from the northern slope backwater surface to the southern center line. In this area, 12, 13, 14, etc. electrode transverse grid line markers were marked with red paint on the top of the dam wave protection wall. Five survey lines were drawn, each consisting of 60 electrodes with 1m spacing on the downstream slope. Due to the challenges of electrode placement on the concrete pavement at the top of the dam, one electrode was omitted to accommodate traffic flow. The remaining electrodes were arranged in a 5 × 5 m uniform grid, see Figure 5, covering an area of 7700 m^2.

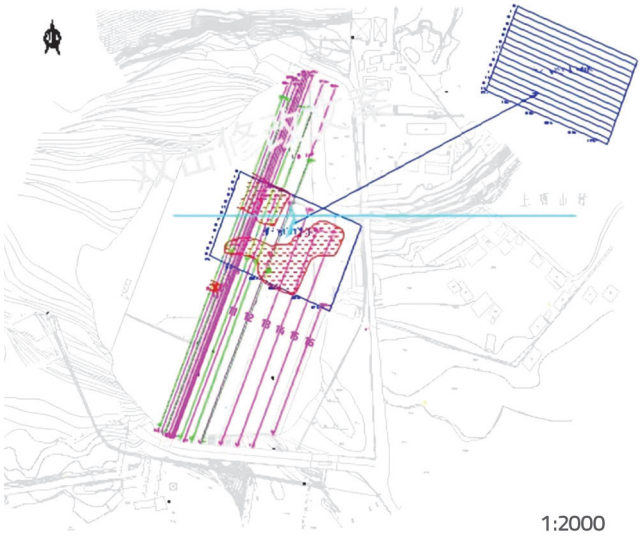

Figure 5. Layout of survey lines

4.3. Test data processing

On-site deployment of the measurement line, electrode smoothing, and automatic grounding resistance testing: The resistance does not meet the grounding conditions required for filler compaction, pouring brine measures to meet the grounding resistance requirements, and implementation of the automatic running pole control measures energised test. After the completion of the test, the scene uses a self-programmed program to collect the original data for 3D resistivity imaging, which reads the data using the extension name of the form . txt to save the orchestration format.

x_1, y_1, z_1, ρ_1
x_2, y_2, z_2, ρ_2
x_3, y_3, z_3, ρ_3
...

where x_i is the horizontal coordinate of the collected electrode points, y_i is the vertical coordinate of the collected electrode points, and zi is the elevation of the corresponding point. The coordinate points are arranged in ascending order, and a comma is used to separate the points from each other.

The 3D high-density electrical survey data of the entire survey area were combined to generate a 3D distribution image of the resistivity for the entire survey area. A 5m spaced slice of the dam resistivity transect is shown in Figure 6, with horizontal distance (m) in horizontal coordinates and elevation (m) in vertical coordinates.

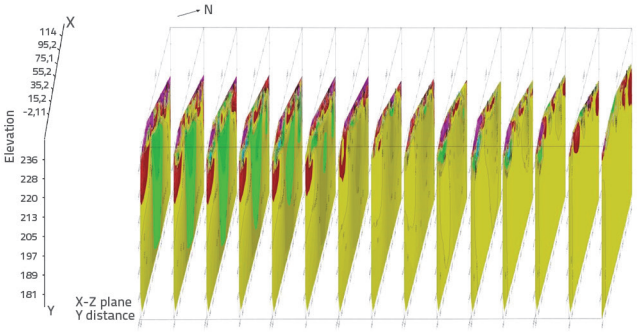

Figure 6. 3D resistivity slice of the measurement area

A convolutional neural network (CNN) was used to annotate scenes in real-time monitoring and identify images with potential hazards. The majority of these images were concentrated in three sections at elevations of 205, 220, and 228 m, which correlated with the estimated locations of possible hazards from the on-site investigations. No screening errors were identified upon manual review of the annotated images after neural network learning.

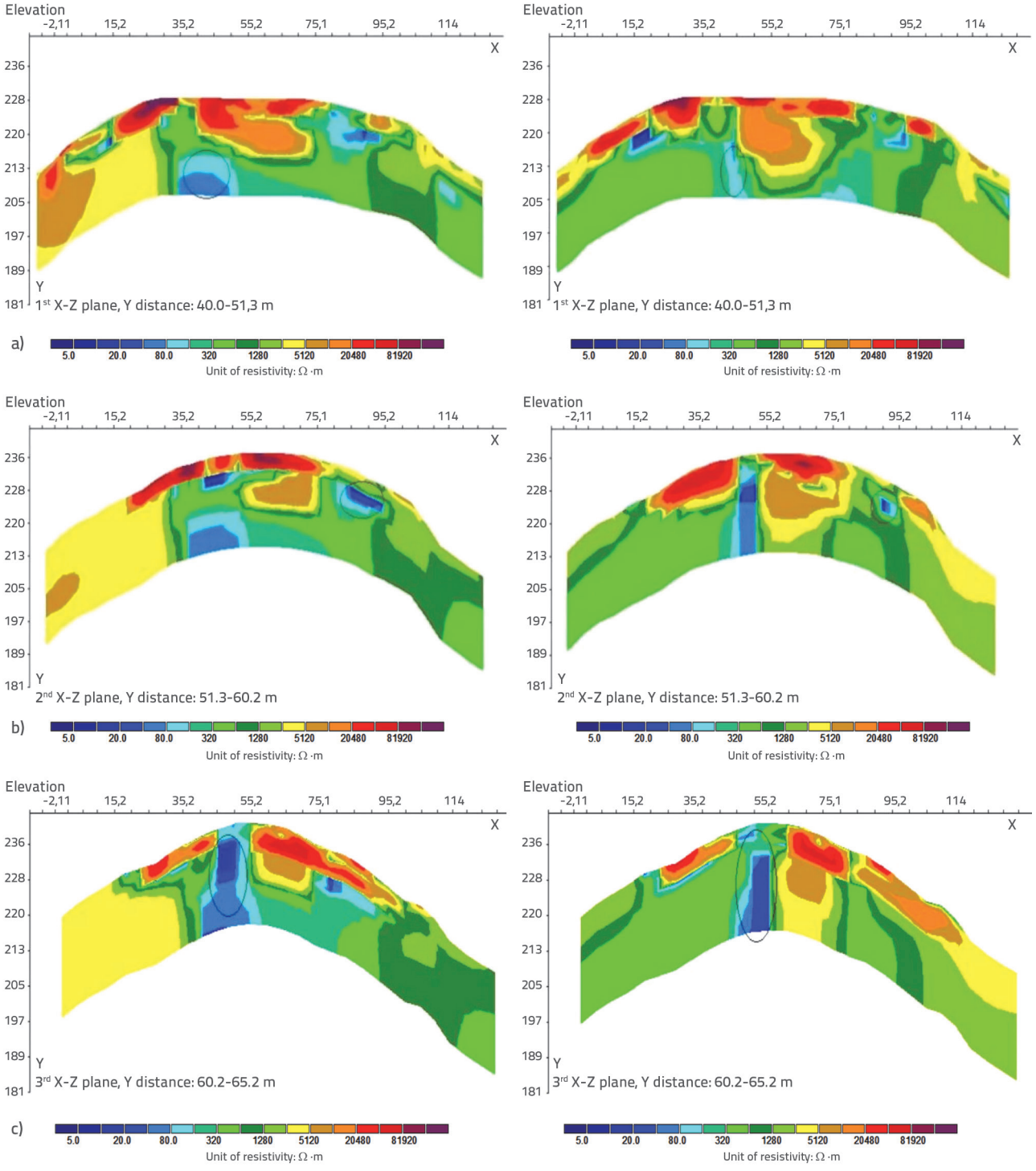

Figure 7. Section slices of sections: a) Section 205 slicing diagram ; b) Section 220 slicing diagram; c) Section 228 slicing diagram

To clearly show the development process of the three sections of 205, 220, and 228 hidden problems, this paper presents the data imaging of the three typical section slice displays. The slice section shown in Figure 7 is a comparison of slices from different recording periods at the same location, where the reason for such a large difference in resistivity values between the two periods in the figure is due to the difference in water content, and this difference does not affect further analysis in this study, with an inverse modelling error of 0.1 %.

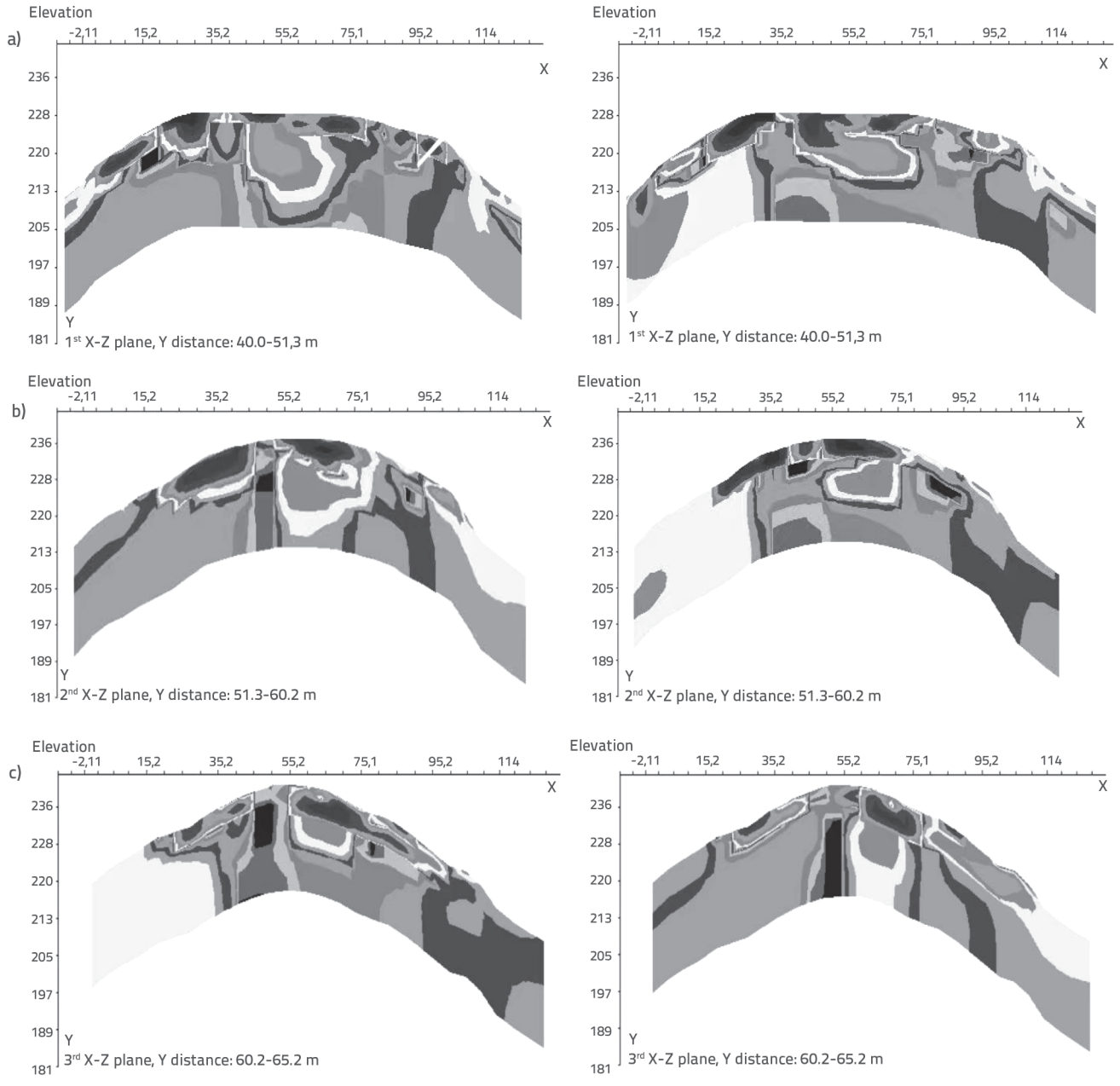

Figure 8. Grey scale processing of sections: a) Section 205, grayscale map; b) Section 220, grayscale map; c) Section 228, grayscale map

4.4. Resistivity image recognition

To further determine the development status of the hidden body in the slice section and to grasp the damage state of the dam material, according to the requirements for the realisation of diagnostic technology, the image recognition method of the seepage damage of the earth and rock embankment dam was used for the image recognition processing of the hidden body.

First, the profiles screening the images containing hidden problems were grayscaled, as shown in Figure 8.

Second, the Canny edge detection algorithm image edge detection[27] results in each colour image boundary map owing to the comparison of the same location. Thus, each section only needs to deal with a map, as shown in Figure 9.

The grayscale processing map was then subjected to Hough straight line detection [28], and the image was cropped to the corresponding position of the region to determine the image calculation region, the results of which are shown in Figure 10.

Spatial colour conversion was performed on the cropped image to convert the image from the RGB colour space into the HSV colour space, and the conversion results are shown in Figure 11.

The colour space converted image was subjected to spatial colour separation, while calculating the pigment threshold of each separated image, the threshold of the original image in

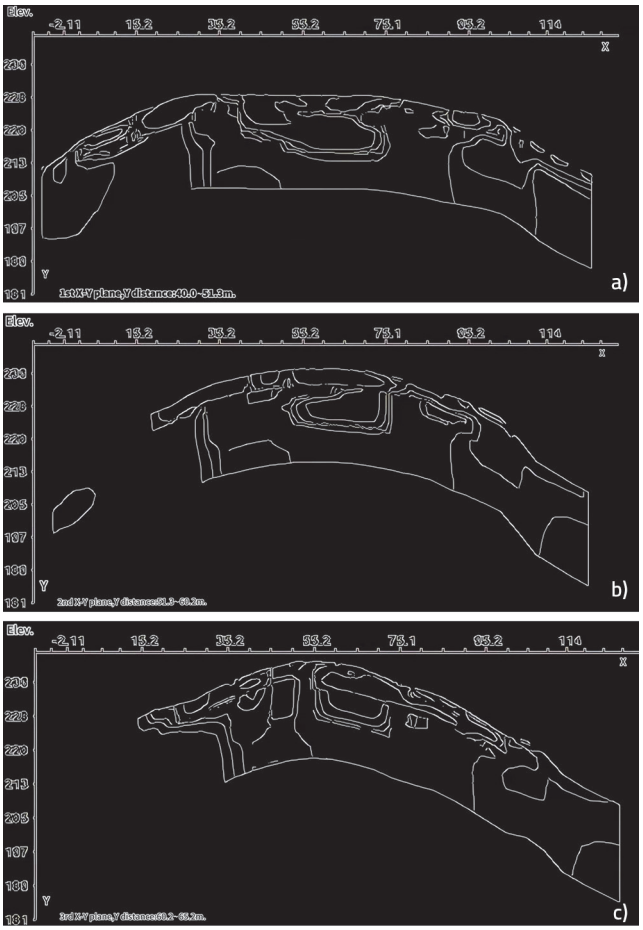

Figure 9. Canny edge detection maps for sections: a) Section 205 - edge detection diagram; b) Section 220 - edge detection diagram; c) Section 228 - edge detection diagram

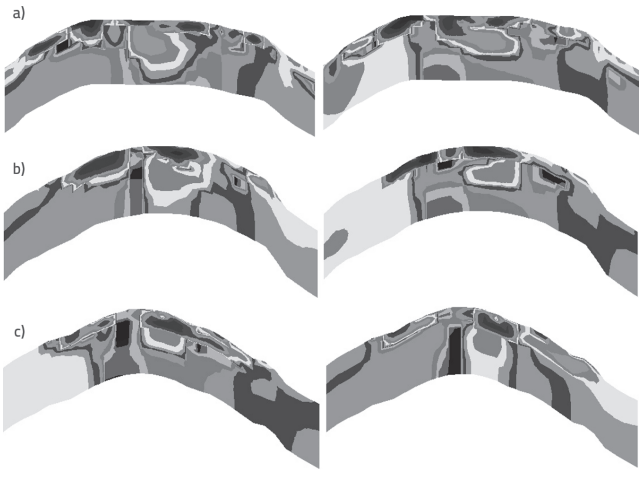

Figure 10. Hough straight-line cut-outs for sections: a) Section 205 - Hough straight cut lines; b) Section 220 - Hough straight cut lines; c) Section 228 - Hough's straight cut lines

the hidden extension area was 103.077, 102.937 and 104.111, respectively, and the results of the spatial colour separation are shown in Figure 12.

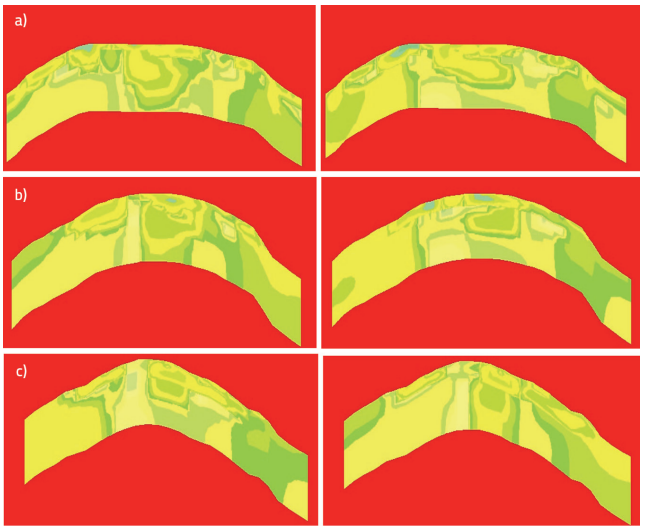

Figure 11. Spatial colour conversion of sections: a) Section 205 - diagram of spatial color conversion; b) Section 220 - diagram of spatial color conversion; c) Section 228 - spatial color conversion diagram

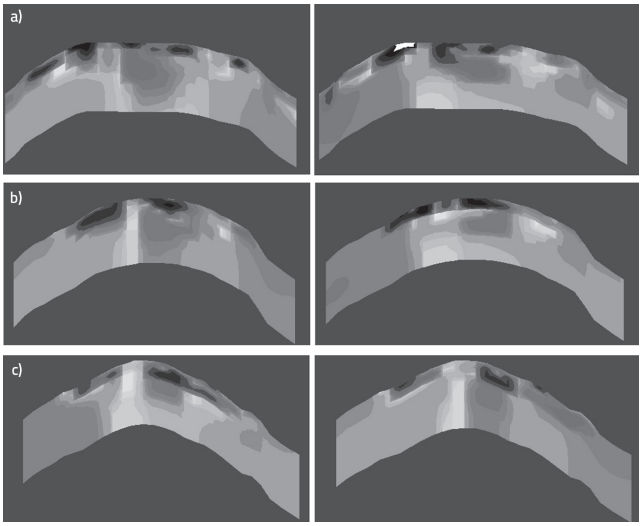

Figure 12. Spatial colour separation of sections: a) Section 205 - diagram of spatial separation of colors; b) Section 220 - color separation diagram; c) Section 228 - diagram of spatial color separation

Finally, the pixel thresholds of the corresponding positions at different moments after spatial colour separation are subtracted to obtain the amount of change in the pigment threshold of the hidden extension area. The values of its 205, 220, and 228 sections are 11.518, 14.736, and 29.773, respectively, and the rate of change of the pigment threshold of the hidden parts of the image can be obtained. The image results are shown in Figure 13.

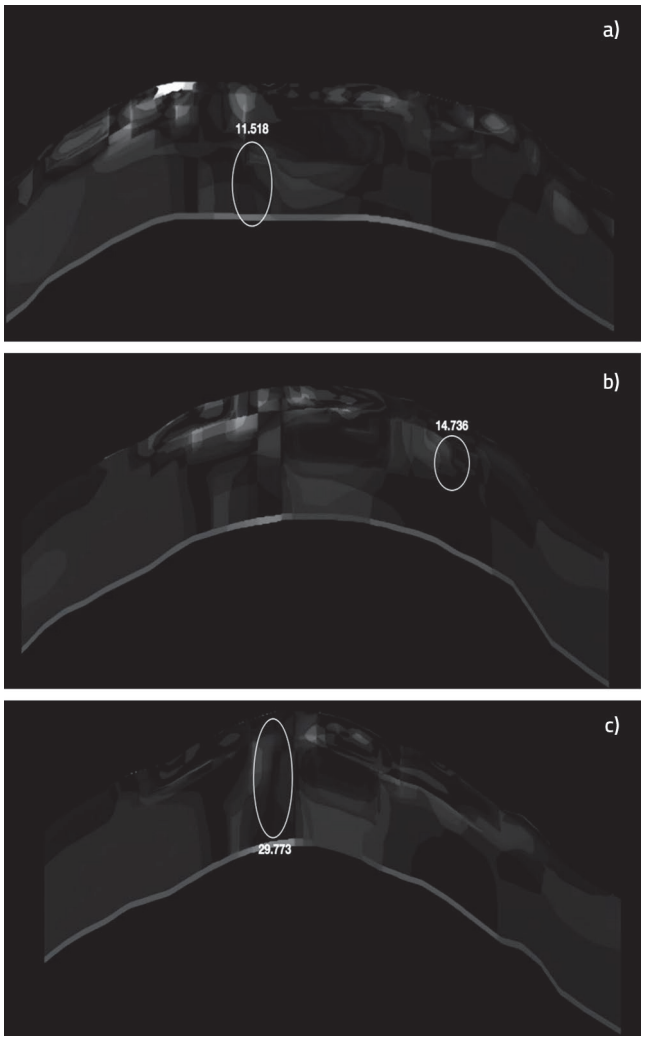

Figure 13. Plot of the results of the phase reduction of the images of sections 205, 220 and 228

5. Leakage diagnosis and evaluation of results

The analysis of resistivity images captured before and after two monitoring sessions at the same location revealed that, using an image comparison recognition algorithm, initial resistivity pigment thresholds of 103.077, 102.937, and 104.111 were identified for the hidden danger area. By calculating the difference in the resistivity thresholds between different time points, the average changes in the resistivity pigment threshold at the same hidden danger location were determined to be 11.518, 14.736, and 29.773. The values of 14.736 and 29.773 were then compared with the pixel threshold at the corresponding position before the expansion of the hidden body to obtain the ratio. The resistivity change rates before and after the two monitoring sessions were 11.1 %, 14.3 %, and 28.6 %. None of these values reached a soil–rock ratio of 7:3. The degree of compaction of the dam body material was 98 %, and the resistivity change rate for the infiltration damage diagnostic conditions was 32.5 %. Based on these data, it is evident that the earth rock dam has not yet experienced seepage deformation failure. However, the rate of change in the electrical resistivity near the northeast corner of the section approached a critical value. The analysis results indicated that this was linked to the observed increase in the seepage water volume during the initial stages. Enhancing monitoring at this specific location and implementing appropriate remedial actions are recommended.

The traditional electrical method for detecting seepage in earth and rock embankment dams can only subjectively determine the location of the hidden body in the seepage field and the approximate scope of damage by the resistivity image formed by the single acquisition data and cannot accurately determine the development status of the hidden body. It was also found that there is no inevitable connection between the low-resistance area in the resistivity image of the earth and rock embankment and whether the dam material reaches the damage of infiltration deformation. This method is very important for the reliability of the input data, so it is important to ensure the accuracy of the data collection and processing. Therefore, compared with the traditional electrical detection, based on 3D RT, not only can we know the deformation and damage state of the earth and rock embankment dam materials in the seepage field at different moments through rapid image comparison, but can also achieve objective and continuous monitoring purposes, and the diagnostic technology is more comprehensive and realistic.

6. Conclusion

In this paper, based on 3D RT imaging technology, we conducted applied research on leakage diagnosis of earth and rock embankment dams based on actual projects. The conclusions of the research are as follows.

The results of the field application demonstrated the feasibility of the processing approach used for the comparative identification of images containing hidden hazards. The findings indicate that initial resistivity pigment thresholds for hazardous areas of the dam body were obtained using an image comparison recognition algorithm. The average change in the resistivity pigment threshold before and after comparing the same potential hazard location was calculated by subtracting the resistivity thresholds at different time points. This value was subsequently compared with the pixel threshold of the corresponding location before the expansion of the potential hazard body. Additionally, the rate of change in the monitored resistance before and after the two time points was analysed to determine the presence of a leakage potential hazard at a specific location.

The application of 3D resistivity imaging technology to the diagnosis of earth and rock dam leakages has shown promising results. By utilising body-rendering image-processing technology, abnormal areas can be more easily identified, allowing for an accurate determination of the evolution of seepage fields within earth and rock embankments at different stages of soil body destruction. In addition, this technology can

effectively display changes in resistivity thresholds, highlighting the expansion of hidden dangers in the region. By reducing the subjective nature of human judgement, this method proved feasible and yielded credible results for the diagnosis of seepage in earth and rock embankment dams.

The analysis of leakage damage in earth and rock embankment dams revealed various hidden dangers that could not be fully addressed using Canny edge detection alone for image comparison. Further research is recommended to explore other image comparison algorithms tailored to specific types of hidden dangers, such as the image centre of mass moving algorithm for dam body slippage and the bubble order algorithm for the random emergence of homogeneous embankment dams. By developing targeted image comparison algorithms, quantitative research on the diagnosis of leakages in earth and rock embankment dams can be conducted.

Acknowledgements

The authors gratefully acknowledge the financial support from the Shandong Provincial Department of Transportation Science and Technology Plan Project (Grant number: 2023B90).

REFERENCES

[1] Alijani-Ardeshir, M., Navayi Neya, B., Ahmadi, M.: Comparative study of various smeared crack models for concrete dams, GRAĐEVINAR, 71 (2019) 4, pp. 305-318, https://doi.org/10.14256/JCE.1540.2015

[2] Chambers, J.E., Wilkinson, P.B., Penn, S., Meldrum, P.I., Kuras, O., Loke, M.H., et al.: River Terrace Sand and Gravel Deposit Reserve Estimation Using Three-Dimensional Electrical Resistivity Tomography for Bedrock Surface Detection, Journal of Applied Geophysics, 93 (2013), pp. 25-32.

[3] Loke, M.H., Barker, R.D.: Rapid Least-Squares Inversion of Apparent Resistivity Pseudosections Using a Quasi-Newton Method, Geophysical Prospecting, 44 (1996), pp. 131-152.

[4] Feng, R., Li, X.Q., Tao, X.L., Sun, C.C., Liu, X.Q., Hao, J.Q.: Electrical Resistivity Tomography for Hydrogeological Exploration, Acta Seismologica Sinica,19 (1997), pp. 655-663

[5] Zhou, J., Wang, F.: Application of High-Density Electrical Resistivity Method in Hidden Hazard Detection of Hongwei Reservoir Earth-Rockfill Dam, Journal of Logistics Engineering University, 24 (2008) 2, pp. 1-5.

[6] Song, W.H.: Discussion on Leakage Detection of Earth-Rockfill Dams Based on High-Density Electrical Method, Dams and Safety, 33 (2013) 1, pp. 38-41.

[7] Zhao, X., et al.: Application of Electrical Resistivity Imaging Technology in Leakage Diagnosis of Earth-Rockfill Dams, Journal of Chongqing Jiaotong University (Natural Science), 28 (2009) 6, pp. 1097-1101.

[8] Zhao, Z., et al.: Experimental Study on Leakage Diagnosis of Earth-Rockfill Dams Based on Temperature Field and Electrical Resistivity Imaging, Journal of Water Resources and Architectural Engineering, 8 (2010) 6, pp. 1-4+27.

[9] Zhao, Y.Z., et al.: Joint Imaging Diagnosis of Leakage in Earth-Rockfill Dams Based on Velocity and Electrical Resistivity (National Natural Science Foundation Project No. 50779081), Chongqing: Chongqing Jiaotong University,2012.

[10] Zhao, W.Y.: Research on Wave-Electric Coupled Imaging Diagnosis Technology for Leakage of Earth-Rock Dams (National Natural Science Foundation Project No.50779081), Research Report of Chongqing Jiaotong University, 2016.

[11] Šunjić, G., Prskalo, M., Milašinović, Z., Harapin, A.: Simulation of concrete ageing on dams as illustrated by numerical analysis of Jablanica HPP, GRAĐEVINAR, 71 (2019) 9, pp. 749-767, https://doi.org/10.14256/JCE.2385.2018

[12] Altunisik, A.C., Sesli, H.: Effect of near-fault ground motion with pulse signal on dynamic response of dam-reservoir-foundation systems, GRAĐEVINAR, 74 (2022) 12, pp. 1059-1083, https://doi.org/10.14256/JCE.1573.2016

[13] Lévy, L., Maurya, P.K., Byrdina, S., et al.: Electrical resistivity tomography and time-domain induced polarization field investigations of geothermal areas at Krafla, Iceland: Comparison to borehole and laboratory frequency-domain electrical observations, Geophysical Journal International, 3 (2024)3

[14] Li, Z.Z.: Application of High-Density Electrical Method in River Crossing Detection in Granite Areas. People's Yellow River, 39 (2017) 5, pp. 109-111.

[15] Liu, P.Y., et al.: Simulation and Application of High-Density Electrical Method in Leakage Monitoring of Dams, Advances in Science and Technology of Water Resources, 41 (2021) 5, pp. 71-75.

[16] Zhou: Preliminary Study on 3D Resistivity Tomography Application. Chinese Journal of Engineering Geophysics, 6 (2009), pp. 549-555.

[17] Johnson, T.C., Burghardt, J., Strickland, C., et al.: 4D proxy imaging of fracture dilation and stress shadowing using electrical resistivity tomography during high pressure injections into a dense rock formation, Journal of Geophysical Research: Solid Earth, 126 (2021) 11, e2021JB022298.

[18] Kawaguchi, T., Saito, T.: Temperature measurement of molten glass under batch feeding process by means of electrical resistance tomography, IOP Publishing Ltd [2024-03-04].

[19] Beff, L., Günther, T., Vandoorne, B., et al.: Three-dimensional monitoring of soil water content in a maize field using Electrical Resistivity Tomography, Hydrology and Earth System Sciences, 17 (2013) 7, pp. 595-609, doi:10.5194/hess-17-595-2013.

[20] Phueakim, K., Amatyakul, P., Vachiratienchai, C.: An attempt to use convolutional neural network to recover layered-earth structure from electrical resistivity tomography survey, IOP Publishing Ltd [2024-03-04].

[21] Rao, G.T., Rao, V.V.S.G., Padalu, G.: Application of electrical resistivity tomography methods for delineation of groundwater contamination and potential zones, Arabian Journal of Geosciences, 7 (2014) 4, pp. 1373-1384.

[22] Zhang, X., Zhao, M., Wang, K., Liu, P., Liu, H.: Application of 3D Electrical Resistivity Tomography for Diagnosing Leakage in Earth Rock-Fill Dam, Engineering, 8 (2016), pp. 269-275.

[23] Li, J.M.: Electric Field and Electric Prospecting. Geological Publishing House, Beijing, 2005.

[24] Yang, J.F., Deng, J.Z., Chen, H.K.H.Y.: 3D Direct Resistivity Forward Modeling by the Precondition Conjugate Gradient Method, Geophysical Geochemical Exploration, 34 (2012), pp. 303-309.

[25] Liu, B., Nie, L.C., Li, S.C. Xu, L., Liu, Z.Y., Song, J., et al.: 3D electrical Resistivity Inversion Tomography with Spatial Constraint, Chinese Journal of Rock Mechanics and Engineering, 31 (2012), pp. 2258-2268.

[26] Song, Y., Li, C., et al.: A parallel Canny edge detection algorithm based on OpenCL acceleration, Plos one, 19 (2024) 1, pp. e0292345.

[27] Uluskan, S.: Automatic detection of regulatory traffic signs via circle detection by post edge detection applied to straight line Hough transform, International Journal of Automotive Science And Technology, 4 (2020) 2, pp. 49-58.